PHYSICAL REVIEW C

NUCLEAR PHYSICS

THIRD SERIES, VOLUME 35, NUMBER 2 FEBRUARY 1987

^{3}He + ^{3}He reaction cross sections at 17.9, 21.7, and 24.0 MeV

Ronald E. Brown
Los Alamos National Laboratory, Los Alamos, New Mexico 87545

F. D. Correll
United States Naval Academy, Annapolis, Maryland 21402

P. M. Hegland*
Department of Physics, University of Pittsburgh, Pittsburgh, Pennsylvania 15213

J. A. Koepke
School of Physics and Astronomy, University of Minnesota, Minneapolis, Minnesota 55455

C. H. Poppe
Lawrence Livermore National Laboratory, Livermore, California 94550
(Received 14 October 1986)

The total reaction cross section σ_R for ^{3}He+^{3}He has been obtained at laboratory bombarding energies of 17.9, 21.7, and 24.0 MeV by measuring the individual cross sections for production of protons, deuterons, tritons, ^{3}He, and α particles. The accuracy of the results is greatly improved by taking advantage of a novel method which depends on the symmetry about 90° in the center-of-mass system of the reaction cross sections for identical particles in the incoming channel. Use of this method reduces the range of energy and angle which must be measured for the continuous spectra of particles emitted in these multibody final states. In order of increasing energy, the values of σ_R obtained in this experiment are 156.7±3.8, 250±14, and 296±12 mb. Individual cross sections contributing to σ_R were also extracted. Implications of the measurements for resonating group calculations of ^{3}He+^{3}He scattering are examined.

I. INTRODUCTION

This paper presents measurements of the total reaction cross section σ_R and the various constituent partial cross sections for the ^{3}He+^{3}He interaction. Measurements were obtained at laboratory bombarding energies of 17.9, 21.7, and 24.0 MeV using a technique which is based on the symmetry of the cross sections about 90° in the center-of-mass (c.m.) system. This technique allowed the total reaction cross section to be determined to an absolute accuracy of about ±5%.

Various approaches have been used to analyze the scattering of light nuclei, including phase-shift decomposition, R-matrix methods, optical model studies, and calculations making use of the resonating group method (RGM).[1–3] Although it is possible to account for open reaction channels by the use of the coupled-channels formalism, it is generally more convenient to introduce complex phase shifts or a phenomenological imaginary potential when the energy exceeds the reaction threshold. With a knowledge of σ_R, one may place constraints on the imaginary parts of the phase shifts or on the imaginary potential, and consequently, various defects in a model calculation may not be able to be compensated by arbitrary adjustments of the imaginary components, and a more stringent test is thereby placed upon the model.

The RGM (Ref. 1–3) has been particularly useful for the study of light systems.[3] This method, which employs a fully antisymmetric wave function and which is based on a realistic nucleon-nucleon force, is often used to generate starting values for phase-shift analyses in order to help avoid spurious phase-shift solutions. Also, it allows for the construction of an effective two-body real potential between the light clusters,[1] which contains the exchange effects produced by the Pauli principle, and therefore the RGM has been extremely important in understanding the results of certain phenomenological optical model analyses. In many of these RGM studies it has been convenient to include the effects of open channels by adding an imaginary potential to the local, direct poten-

tial[4–7] (although some calculations have introduced the imaginary part into the nonlocal kernel[8]). In general, the parameters of the imaginary potential have been determined by fitting phase shifts, if a complex phase shift analysis is available, or by fitting the elastic differential cross sections.

Guided by the original work with ^{4}He+^{4}He scattering,[4] RGM studies of other systems seem to indicate that the phenomenological imaginary potential may be described by a sum of volume and surface forms (typically a Woods-Saxon form and its derivative) of equal strength with energy-independent geometrical parameters. The latter parameters are chosen to yield a mean-square radius for the potential which is approximately equal to that for the direct nuclear potential. The strength of the potential required to fit the elastic data is found typically to vary smoothly with energy.

When an effective two-body real potential is derived from an RGM calculation, the combined effect of the Pauli principle and the exchange nature of the nucleon-nucleon force appears as a Majorana component in this real, local potential.[9] That is, the effective potential may be written

$$V^{\text{eff}}=\alpha(1+\beta P^r)V_D \ ,$$

where α and β are constants, V_D is the direct (folded) potential, and P^r is the space-exchange operator which exchanges the c.m. coordinates of the two interacting clusters. Such a Majorana operator gives rise to a factor of $(-1)^l$ when a partial-wave expansion is made and produces an odd-even effect, for example, on the calculated phase shifts. It is tempting, therefore, to ascribe a similar property to the phenomenological absorptive potential[5] and, consequently, in many analyses the potential iW has appeared with

$$W(r)=[1+C_I(-1)^l]U(r) \ , \tag{1}$$

where

$$U(r)=-U_0\left\{\frac{1}{1+\exp\left[\dfrac{r-R}{a}\right]}+\frac{4\exp\left[\dfrac{r-R}{a}\right]}{\left[1+\exp\left[\dfrac{r-R}{a}\right]\right]^2}\right\}, \tag{2}$$

U_0 and C_I being adjustable parameters. Including C_I was originally found to improve fits to the p + ^{4}He scattering data,[5] and more recently such an odd-even effect was introduced into studies of d + d (Ref. 6), ^{3}He + ^{4}He (Ref. 10), and ^{3}He + ^{3}He (Refs. 11 and 12) scattering.

Some measurements of σ_R have been made for the cases mentioned above, in order to study the effect of W more carefully. Using the anticoincidence beam-attenuation technique Sourkes *et al.*[13] measured σ_R for p + ^{4}He at 16 energies. Their measured cross sections were found to be substantially smaller than those predicted by an optical model fit[14] to elastic scattering data in the same energy range. When it was required[14] that the optical-model imaginary potential produce smaller σ_R values, the fit to the elastic data was worsened significantly. On the other hand, the RGM calculations[13] were able to reproduce both the elastic and σ_R data by adjusting U_0 and using the negative values for C_I determined in Ref. 5 from fits to the elastic data only. The negative values for C_I indicate that W is stronger in odd-l than in even-l states.

Measurements of σ_R at a single energy have been made for d + d (Ref. 15) and ^{3}He+^{4}He (Ref. 16) by summing up the partial cross sections. For the d + d case RGM calculations[6] based on fits to elastic data only required an odd-even effect in W in order to get good fits to the differential cross section near 90° (c.m.). Similar calculations were repeated at 17.5 MeV,[17] but with the inclusion of Coulomb exchange, and reasonable agreement with the measured value for σ_R was obtained.[2,15] Such agreement was not obtained, however, for ^{3}He+^{4}He (Ref. 16) at 27.9 MeV, where the measured value (433±10) mb did not agree with the RGM values (285±40) mb. Those calculations do indicate a rapid change in σ_R with energy, reaching the measured value at higher energies. It is possible that some missing feature of the calculation has caused a shift in energy and that agreement between measurement and calculation is better than it appears. However, when a phase shift analysis of the elastic scattering is performed[16] using the measured σ_R as a constraint on the imaginary part of the phase shift, the presence of the odd-even effect is not at all clear. In the RGM calculation, which is used as a starting point for the phase shift analysis, the odd-even effect is built in because of the form of W. As for the p + ^{4}He case,[5] the RGM calculations for d + d (Refs. 6 and 15) and ^{3}He+^{4}He (Refs. 10 and 16) infer a negative value for C_I. Clearly, more data and analysis are needed before this exchange effect in the absorption can be definitely established.

The ^{3}He+^{3}He interaction requires that absorption be accounted for at all scattering energies because the reaction ^{3}He+^{3}He→^{4}He + p + p is exoergic. This was addressed by again including an imaginary potential of the form of Eqs. (1) and (2) into an RGM calculation.[11,12] In the energy range 3.0—17.9 MeV, σ_R data[18] were available in addition to elastic differential cross sections, and so U_0 and C_I were determined by requiring that the calculations reproduce the measured σ_R. These cross sections, obtained by Bacher by measuring the charge-1 particles as discussed in Sec. II A, increase smoothly from 3.0 to 15.9 MeV and require a value for U_0 which increases from 0.12 MeV to only 0.2 MeV. The value of the odd-even parameter, C_I, required to fit these data is consistent with zero. At the next energy where a measurement exists, 17.9 MeV, σ_R exhibits a marked increase from its value at lower energies and U_0 reflects this increase; C_I remains consistent with zero. Because ^{3}He+^{3}He elastic differential cross section measurements exist as high as 74.8 MeV, the RGM calculations of Ref. 12 were extended past the region where σ_R measurements existed by using U_0 and C_I as adjustable parameters and minimizing χ^2 in a fit to the elastic cross sections. The result was that the strong increase in U_0 observed between 15.9 and 17.9 MeV continued, with U_0 approaching 3 MeV at 74.8 MeV incident

energy. In this energy range where σ_R measurements did not exist, a positive value of C_I ranging from 0.27 to 0.55 was required to fit the data. Using the parameters extracted from the RGM fits to the elastic data, the predicted σ_R was found to continue the rapid rise from 15.9 MeV, leveling off at a value of about 780 mb at 54.8 MeV (see Fig. 8). This predicted σ_R is considerably larger than that for any of the other light systems mentioned above.

In order to better understand the ^{3}He+^{3}He interaction, we have extended the σ_R measurements to 24 MeV. This is in the region where the RGM predictions[12] are increasing most rapidly. Because the onset of this rapid increase was apparently indicated by the highest energy measurement of Bacher,[18] we also have repeated a measurement at this energy. However, our technique differs from that of Ref. 18 and allows for a separate determination of the individual reaction cross sections. Consequently, we hoped to uncover how the partial cross sections contributed to σ_R and which ones might be responsible for the rapid increase with energy. We shall show that our measurements do not support the 17.9 MeV datum of Ref. 18 and are not in agreement with the RGM predictions of Ref. 12.

II. DETERMINATION OF REACTION CROSS SECTIONS

A. Cross section relations

We have determined the ^{3}He+^{3}He total reaction cross section σ_R by measuring the partial cross sections which comprise it. Although it may be possible to measure σ_R by applying the beam attenuation technique such as used by Sourkes *et al.*[13] for p + ^{4}He and p + ^{3}He, the elastic scattering corrections become very large at lower energies and, more importantly, one cannot distinguish the various components of σ_R. In Table I we list all the possible ^{3}He + ^{3}He reactions which can occur, their Q values, and their threshold energies. As an example of the notation in the table, 2p2d indicates that two protons and two deuterons are produced in the final state. We observe that all the reactions produce at least three particles, thereby yielding continuous energy distributions for each reaction product. The total reaction cross section is the sum of all partial reaction cross sections, integrated over the continuous energy distributions and over a 4π solid angle.

When many competing multibody reaction channels are open, it is not possible in general to measure the cross section for a given reaction without making use of coincidence techniques. A much simpler measurement is that of σ_x, the total cross section for the production of particle x. In terms of the different final states listed in Table I, the cross sections for the production of every particle from the interaction of ^{3}He and ^{3}He may be written

$$\begin{aligned}
\sigma_n &= \sigma(2pn\,{}^3He) + \sigma(3pnd) + 2\sigma(4p2n)\,, \\
\sigma_p &= 2\sigma(2p\alpha) + \sigma(pd\,{}^3He) + 3\sigma(3pt) + 2\sigma(2pn\,{}^3He) \\
&\quad + 2\sigma(2p2d) + 3\sigma(3pnd) + 4\sigma(4p2n)\,, \\
\sigma_d &= \sigma(pd\,{}^3He) + 2\sigma(2p2d) + \sigma(3pnd)\,, \\
\sigma_t &= \sigma(3pt)\,, \\
\sigma_{^3He} &= \sigma(pd\,{}^3He) + \sigma(2pn\,{}^3He)\,, \\
\sigma_\alpha &= \sigma(2p\alpha)\,.
\end{aligned}$$

The notation is as in Table I, e.g., $\sigma(2p\alpha)$ is the cross section for the ^{3}He+^{3}He$\rightarrow\alpha$+p + p reaction. It follows from the above expressions that σ_R can be expressed in terms of the production cross sections by the relation

$$\sigma_R = \tfrac{1}{4}(\sigma_p + \sigma_d + \sigma_t) + \tfrac{1}{2}(\sigma_\alpha + \sigma_{^3He})\,. \tag{3}$$

It is evident from this expression that σ_R may be measured at all energies by measuring the production of charged particles only, thereby avoiding the complication of neutron detection.

Below the 2p2d threshold (21.94 MeV) a simplification occurs, and the expression for σ_R becomes

$$\sigma_R = \sigma_\alpha + \sigma_t + \sigma_{^3He}\,, \tag{4}$$

so that one need only detect the three kinds of particles indicated. However, if deuterons are also detected the individual reaction cross sections below the 2p2d threshold may be determined according to

$$\begin{aligned}
&\sigma(2p\alpha) = \sigma_\alpha\,, \\
&\sigma(pd\,{}^3He) = \sigma_d\,, \\
&\sigma(3pt) = \sigma_t\,, \\
&\sigma(2pn\,{}^3He) = \sigma_{^3He} - \sigma_d\,.
\end{aligned} \tag{5}$$

Between 21.95 and 26.39 MeV (the 3pnd threshold) the individual cross sections may also be obtained, provided one now detects protons as well. In this range the reaction cross sections are related to the particle production cross sections by the following relations:

$$\begin{aligned}
&\sigma(2p\alpha) = \sigma_\alpha\,, \\
&\sigma(pd\,{}^3He) = \sigma_{^3He} - \tfrac{1}{2}(\sigma_p - 2\sigma_\alpha - 3\sigma_t - \sigma_d)\,, \\
&\sigma(3pt) = \sigma_t\,, \\
&\sigma(2pn\,{}^3He) = \tfrac{1}{2}(\sigma_p - 2\sigma_\alpha - 3\sigma_t - \sigma_d)\,, \\
&\sigma(2p2d) = \tfrac{1}{2}(\sigma_d - \sigma_{^3He}) + \tfrac{1}{4}(\sigma_p - 2\sigma_\alpha - 3\sigma_t - \sigma_d)\,.
\end{aligned} \tag{6}$$

Above 26.39 MeV the individual cross sections cannot be determined unless neutrons are detected, and above

TABLE I. Q values (MeV) and laboratory threshold energies (MeV) for ^{3}He+^{3}He reactions.

Final state	Q	Threshold
2pα	12.85	
pd ^{3}He	−5.50	10.98
3pt	−6.97	13.92
2pn ^{3}He	−7.73	15.44
2p2d	−10.99	21.94
3pnd	−13.23	26.39
4p2n	−15.46	30.84

30.84 MeV it is not possible to determine the individual cross sections unless coincidence techniques are used. Nevertheless, σ_R may be determined from Eq. (3) at any energy.

By algebraic manipulation, an alternate form for Eq. (4) is found to be

$$\sigma_R = \tfrac{1}{2}(\sigma_p + \sigma_d - \sigma_t) , \tag{7}$$

which is valid below 21.94 MeV. Thus if the cross section for the production of tritons is negligible compared to that for protons and deuterons, or if the energy is less than the 3pt threshold, then one may obtain σ_R by detecting only protons and deuterons. This is what was done by Bacher[18]—the conditions described above for the tritons were met in the energy range spanned by his measurements.

B. The E^* method

In order to determine a given σ_x, one would, in general, measure the continuous energy spectrum for particle x at a given laboratory angle and integrate this spectrum from the maximum energy down to as low an energy as possible. Such integrated spectra must then be obtained over as wide an angular range as possible in order that the integration over solid angle may be made. Experimental limitations imposed on both the energy and angular range of the detected particles are the largest source of uncertainty in determining σ_R by this technique. For example, the particle telescope used to identify the different reaction products imposes a lower cutoff of about 1 MeV to the energy spectrum, associated largely with the energy of those particles whose range equals the thickness of the ΔE detector. The size of the telescope may prevent very large or very small angles from being reached. These inaccessible regions of energy-angle space may contribute a significant amount to σ_R and a way must be found to correct, avoid, or compensate for this deficiency. In Ref. 16 the problem was treated for the ^{3}He+^{4}He reaction by fitting a reaction model to the measured energy spectra as a function of angle. The model calculations were then used to extrapolate in energy and angle, thereby increasing the confidence with which both the energy and angular integrations were made.

In Ref. 15 for the d + d reactions, a very elegant technique was used which depends upon the symmetry about 90° (c.m.) of the reaction cross sections for the interaction of identical particles. The technique is referred to as the "E^* method," and is now described.

If we let $\sigma_i^{\text{c.m.}}(\theta^{\text{c.m.}}, E^{\text{c.m.}})$ be the c.m. cross section for the ith reaction, where the detected particle is emitted in the c.m. system at an angle $\theta^{\text{c.m.}}$ with an energy $E^{\text{c.m.}}$, then the total cross section σ_i for this reaction is given by

$$\sigma_i = 2\pi \int_0^{\pi} \int_0^{E^{\text{c.m.}}_{\max}} \sigma_i^{\text{c.m.}}(\theta^{\text{c.m.}}, E^{\text{c.m.}}) \times \sin\theta^{\text{c.m.}}\, dE^{\text{c.m.}}\, d\theta^{\text{c.m.}} .$$

Because of the identity of projectile and target one has

$$\sigma_i^{\text{c.m.}}(\theta^{\text{c.m.}}, E^{\text{c.m.}}) = \sigma_i^{\text{c.m.}}(\pi - \theta^{\text{c.m.}}, E^{\text{c.m.}}) ,$$

so it follows that

$$\sigma_i = 4\pi \int_0^{\pi/2} \int_0^{E^{\text{c.m.}}_{\max}} \sigma_i^{\text{c.m.}}(\theta^{\text{c.m.}}, E^{\text{c.m.}}) \times \sin\theta^{\text{c.m.}}\, dE^{\text{c.m.}}\, d\theta^{\text{c.m.}} . \tag{8}$$

The limits of integration are indicated in Fig. 1(a), which illustrates a typical nonrelativistic transformation between the laboratory and c.m. coordinates. [This particular illustration happens to be for the kinematic case where a maximum lab angle (a cone angle) exists, which is realized for many of the reactions considered at the energies studied here; the arguments are also valid when the maximum

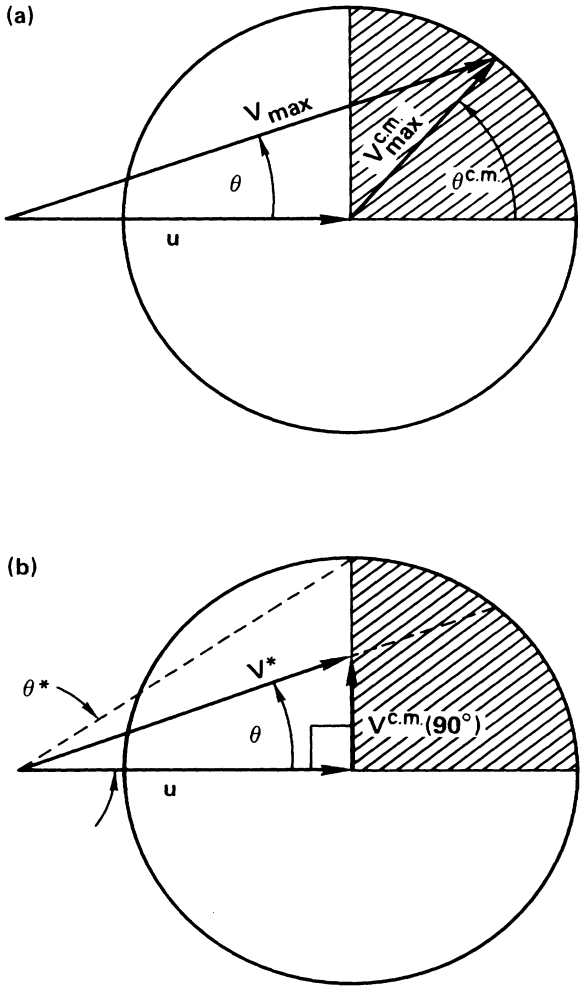

FIG. 1. (a) Laboratory to center-of-mass transformation diagram. The limits of integration for Eq. (8) are spanned by the shaded quadrant for a reaction which produces three or more particles in the final state. The maximum possible velocity for such a reaction is $v_{\max}^{\text{c.m.}}$ in the c.m. system. (b) The same limits of integration are obtained in the laboratory system by integrating the laboratory velocity between v^* and $v_{\max}$ and θ between 0° and θ^*. v^* is that velocity at angle θ corresponding to particles emitted at 90° in the c.m. system.

laboratory angle is equal to π.] For a reaction which produces three or more particles in the final state, the c.m. velocity of the detected particle varies from some maximum $v_{\max}^{\text{c.m.}}$ down to zero, so that for Eq. (8) the limits of integration span the first quadrant of the circle, shown shaded in Fig. 1(a). In the laboratory frame, Eq. (8) becomes

$$\sigma_i = 4\pi \int_0^{\theta^*} \int_{E^*}^{E_{\max}} \sigma_i(\theta,E)\sin\theta \, dE \, d\theta \, , \tag{9}$$

so that, as illustrated in Fig. 1, at a given laboratory angle θ, one integrates from a maximum energy $E_{\max}$ (corresponding to velocity $v_{\max}$) down to a minimum energy E^* which corresponds to the laboratory velocity v^* at which the detected particles are emitted at 90° in the c.m. system [see Fig. 1(b)]. The laboratory angular range then lies between 0 and θ^*, where $\tan\theta^* = v_{\text{c.m.}}^{\max}/u$, and u is the velocity of the c.m. system with respect to the lab system. At a given lab angle, one has, nonrelativistically,

$$E^* = \tfrac{1}{2} M_x v^{*2} = \frac{M_x E_b}{4M\cos^2\theta} \, , \tag{10}$$

where M_x is the mass of the detected particle, M is the mass of the target or projectile, and E_b is the projectile laboratory energy. Consequently, the energy E^* at a given angle and incident energy depends only on the mass of the detected particle *and not on the reaction producing it.*[19] This is crucial for the E^* method and means that, although several different reactions may contribute to a specific particle spectrum, there is only one lower limit E^* for that particle type, and all particles of that type may be detected and integrated together without the need for a coincidence measurement to identify a particular reaction. This independence of the reaction type does not hold for the angular limit θ^*, which does depend on the reaction Q value, i.e., $v_{\max}^{\text{c.m.}}$ depends on Q. However, this is of no consequence, for if one integrates each spectrum down to E^*, then once θ^* is reached for a given reaction, that reaction no longer contributes to the integral—one simply integrates in angle out to the largest value $\theta_{\max}^*$ of θ^* for all reactions which can produce particles of a given type. In Eq. (9) then, we replace the cross section σ_i for a given reaction with the production cross section for particle x, i.e.,

$$\sigma_x = 4\pi \int_0^{\theta^*_{\max}} \int_{E^*}^{E_{\max}} \sigma_x(\theta,E)\sin\theta \, dE \, d\theta \, . \tag{11}$$

Therefore the experiment consists in measuring the spectrum $\sigma_x(\theta,E)$ for each different particle x for laboratory angles out to $\theta_{\max}^*$ and integrating these spectra down to a lower limit $E^*(\theta)$. This E^* method greatly reduces the energy and angular ranges that must be spanned and therefore increases the accuracy with which σ_R may be determined.

III. EXPERIMENTAL METHODS

Initial data for this experiment were obtained at the Williams Laboratory of the University of Minnesota using the model MP tandem Van de Graaff accelerator. Somewhat later the experiment was completed using the FN tandem Van de Graaff at the ion beam facility of the Los Alamos National Laboratory. The techniques used at both laboratories were identical, although physically different detector systems were used.

Because of the simplifications that exist at energies below the 2p2d threshold at 21.94 MeV [see Eqs. (4) and (5)] the initial bombarding energy chosen was 21.7 MeV. In order to detect deuterons, tritons, ^{3}He particles, and α particles, a three-detector telescope was assembled consisting of Si surface-barrier detectors of thicknesses 24, 48, and 700 μm. To detect ^{3}He and α particles, the 24-μm detector was used as a ΔE detector and the 48- and 700-μm detectors were used together as the stopping detector. Standard particle identification techniques were used. Deuterons and tritons were detected in the same telescope by using the 24- and 48-μm detectors together as a 72-μm ΔE detector and the 700-μm detector as the stopping detector.

The target gas, 99.9% pure ^{3}He at about 400 Torr, was contained in a 23.9-mm diameter cylindrical gas cell with a 6.3-μm Kapton foil window located at the center of an evacuated scattering chamber. Other experimental details are similar to those previously reported.[16]

Pulse-height spectra of tritons, deuterons, ^{3}He and α particles obtained using the system described above are shown in Fig. 2 at 21.7 MeV and a laboratory angle of 15°. For each spectrum the maximum particle energy for the different reactions is indicated by arrows labeled according to the particular final state. The energies E^* for which the detected particles are emitted at 90° (c.m.) are also indicated. At forward angles a few cases were observed where the instrumental cutoff in a spectrum was a few channels higher than E^*, as illustrated by the ^{3}He and deuteron spectra of Fig. 2, necessitating a minor extrapolation. In all such cases the error introduced by such an extrapolation was negligible, and at larger angles this problem was not encountered because of the increase of E^* with angle [see Eq. (10)].

Because the accuracy with which σ_R can be determined by this method depends on knowing where E^* occurs in each spectrum, it is important that an accurate energy calibration be made. This was accomplished by putting deuterium gas into the target cell and measuring, as a function of angle, the pulse height of scattered ^{3}He, recoil deuterons, and α particles from the $^3\text{He} + \text{d} \rightarrow \alpha + \text{p}$ reaction. The known kinematics of these monoenergetic particles allowed for an accurate calibration of the ^{3}He, deuteron, and α particle spectra. Because tritons and deuterons are detected simultaneously in the same ΔE-E arrangement, it was assumed that the triton energy calibration was the same as that measured for the deuterons. This is corroborated by observing that the ^{3}He and α particle energy calibrations were identical. Figure 2 also shows the $^3\text{He}+^3\text{He}$ elastic scattering peak. The presence of this peak allowed a check on the energy calibration and, by comparing the elastic yields with previously measured cross sections, it was possible to check the determination of the absolute reaction cross sections. The low energy tail of the elastic peak, produced by slit scattering, contributes in the region of the ^{3}He continuum. Corrections applied for this and other effects will be discussed below.

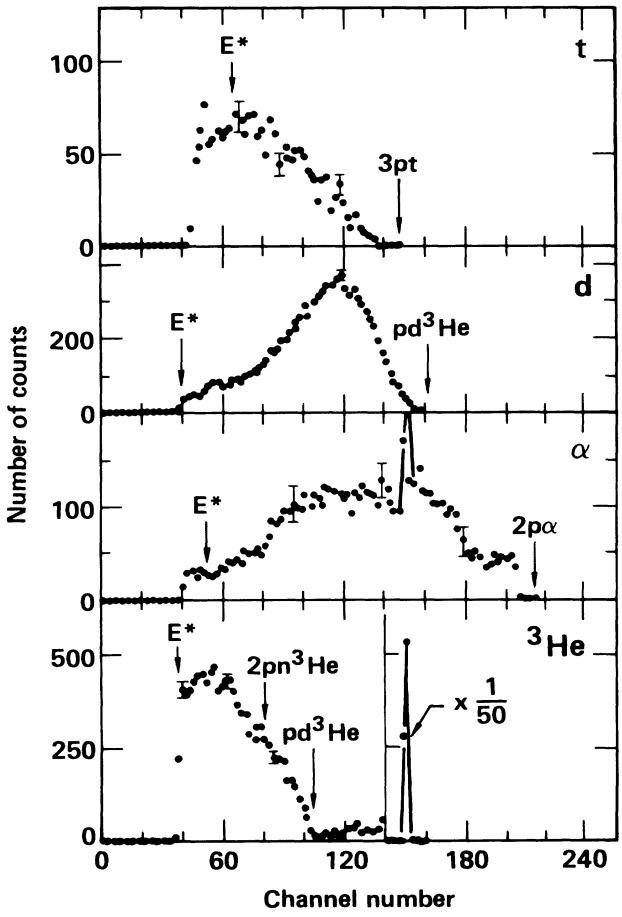

FIG. 2. Pulse-height spectra for tritons, deuterons, α particles, and ^{3}He particles emitted at 15° from ^{3}He+^{3}He at 21.7 MeV. The energy E^* at which the detected particle is emitted at 90° in the c.m. frame is indicated by the arrow. Other arrows indicate the maximum possible energy for various three-or-more-body reactions.

The large yield of elastic ^{3}He particles caused some electronic leakage into the α-particle spectrum, which is observed in Fig. 2 as a sharp peak on the α-particle continuum. This leakage contribution is easily subtracted from the α-particle yield. The shelf appearing at the high energy end of the α-particle spectrum is real, being caused by the virtual state of the diproton. The error bars in Fig. 2 represent counting statistics only.

Preliminary analysis of the 21.7-MeV data yielded a value for σ_R significantly less than Bacher's result[18] at 17.9 MeV. We therefore repeated the measurement at this lower energy and found a value about one-half of that reported in Ref. 18. In order to locate the source of this large discrepancy, we decided to measure the proton spectra at 17.9 MeV. There were three reasons for doing this: (1) We would be measuring σ_R in a manner closely related to the method of Ref. 18; (2) we would have an independent check on our method [i.e., Eq. (7) vs Eq. (4)]; (3) we would develop the technique needed for obtaining σ_R and the partial cross sections above 21.9 MeV [Eq. (3)].

In order to address points (1) and (2) above, we intended to measure σ_p, the proton production cross section, and add to it our previously measured value for σ_d. Because our measurements at 17.9 MeV had indicated that σ_t was negligible, this sum yields directly σ_R according to Eq. (7). We can still use the E^* method for protons in order to increase the accuracy in integrating the spectra and to greatly reduce the angular range over which data need be taken (at 17.9 MeV, θ^* is 72.4°). Because of the large positive Q value (12.85 MeV) of the ^{3}He+^{3}He$\rightarrow\alpha$+p+p reaction and the fact that E^* for protons is much lower than for any other particle, the dynamic range required for identifying protons is very large—from about 1.5 to 30 MeV at 10°. In order to accommodate this range, we used a three-detector telescope consisting of 100- and 250-μm surface barrier transmission detectors and a 5-mm, Li-drifted stopping detector. When the first detector (100 μm) is used as the ΔE detector and the 250-μm and 5-mm detectors together are used as the stopping detector, the lower energy portion of the proton energy range can be covered with the particle identification system. In another mode in which the 100- and 250-μm detectors form the ΔE detector, the upper portion of the range is covered. Switching between modes was done automatically by a logic signal derived from the energy loss signal of the 100-μm detector. Energy calibration of the proton detector was accomplished by filling the target cell with H_2 or D_2 and measuring the pulse height of the recoil protons and deuterons from ^{3}He bombardment.

Proton spectra obtained with this detector system were compared with those of Ref. 18. The spectra are dominated at the high energy end by a sharp peak corresponding to protons from ^{3}He+^{3}He$\rightarrow^5$Li + p. (Figure 3 shows

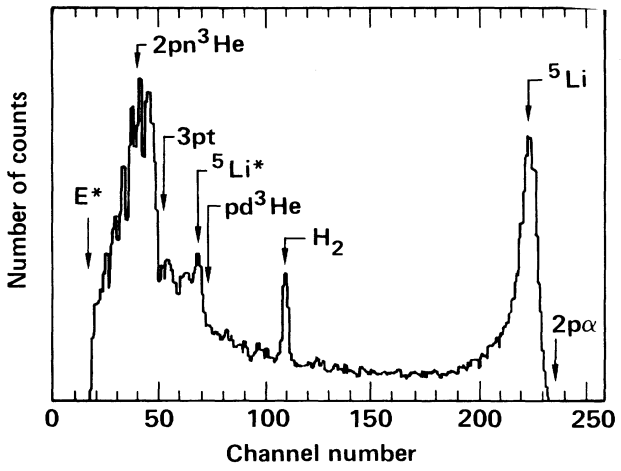

FIG. 3. Pulse-height spectrum for protons emitted at 20° from ^{3}He+^{3}He at 17.9 MeV. The energy E^* at which protons are emitted at 90° in the c.m. frame is indicated by the arrow. Other arrows indicate the energy of protons which leave ^{5}Li in its ground state and second excited state at 16.65 MeV as well as the maximum possible energy for various multibody reactions. The arrow labeled H_2 corresponds to recoil protons from an H_2 contaminant in the target gas.

an example of such a spectrum obtained, however, at Los Alamos.) Below this peak, our spectra level off, remaining flat down to very low energies where the yield again rises, presumably because of protons from the decay of unstable ^{5}Li and from competing breakup reactions. In Ref. 18, however, a broad peak occurs in the middle of the spectra. This peak is not observed in any of our spectra, and its origin remains unknown. We did, however, observe a small, narrow peak in that intermediate region which was traced to recoil protons from a small amount of H_2 contamination in the target gas. The area of this peak is only a small fraction of that which appears in the Ref. 18 spectra and was subtracted before our data were integrated. The value for σ_R extracted from these proton measurements and the previous deuteron spectra yielded a value for σ_R about 15% greater than that which we obtained earlier from the ^{3}He, α-particle, and triton measurements. This disagreement was subsequently traced at Los Alamos to having been caused by insufficient thickness of some of the antiscattering slits in the proton detector telescope assembly. Consequently, we conclude that our earlier results for σ_R are confirmed by the measurement using protons, and we attribute the difference between our measurements and the results of Ref. 18 to the presence of a large contamination, of unknown origin, in the Ref. 18 spectra.

Preliminary measurements of deuteron and triton production cross sections were obtained at Minnesota at 24 MeV; however, the experiment was completed at Los Alamos where protons, deuterons, tritons, ^{3}He, and α particles were measured at 17.9 MeV again and at 24 MeV. The detector telescopes used at Los Alamos were similar to those used at Minnesota: for deuterons, tritons, ^{3}He, and α particles, surface barrier detectors of 17 and 40 μm were used along with a 1000-μm Li-drifted stopping detector; for protons 25- and 220-μm surface barrier detectors were combined with a 5-mm Li-drifted detector. As before, the appropriate combination of transmission detectors was used to distinguish ^{3}He and α particles ($\Delta E = 17$ μm) from deuterons and tritons ($\Delta E = 17$ μm + 40 μm). For the proton telescope, however, it was found that by summing the two transmission detectors to form a ΔE detector of 245 μm, we were able to span the entire proton range at both 17.9 and 24 MeV.

Various corrections were applied to the data before the final cross sections were extracted. In order to correct the ^{3}He continuum for the low energy tail on the elastic peak produced by slit scattering (see Fig. 2), the target cell was filled with ^{4}He gas and the spectrum of ^{3}He scattered by ^{4}He was measured. Because no continuum is produced in this case one can measure the number of slit-scattered ^{3}He particles in the appropriate energy range and correct the ^{3}He + ^{3}He data accordingly. It was found, however, that a much simpler and equally accurate method was to subtract a linear background under the ^{3}He continuum by extrapolating from the region between the continuum and the elastic peak. This latter method was used in the Los Alamos runs. At very forward angles, background produced by the cell window can contribute to the spectra. This was easily corrected by taking runs with the target cell evacuated.

At the most forward angles the collimator assembly on the detector may interfere somewhat with the edges of the beam transmitted through the target cell, thereby slightly altering the integration of the beam current. This problem is worse at the lowest energy (17.9 MeV) where there is more multiple scattering of the beam as it passes through the target. At Minnesota a fixed detector, which monitored ^{3}He elastic scattering, was used to make corrections ($\lesssim 10\%$) for this problem. For the Los Alamos runs, however, no fixed detector was used and the data at the forwardmost angles were corrected by comparison with the Minnesota data, where such existed (all except p, ^{3}He, and α spectra at 24 MeV) or were discarded (typically only measurements at 13°).

Contamination of the ^{3}He gas was also investigated as a possible source of error. Figure 3 shows the 17.9-MeV proton spectrum at 20° obtained at Los Alamos. The peak in the spectrum near channel 100 was identified by its energy and behavior with angle as being elastic recoil protons from an H_2 contaminant. From the known p + ^{3}He elastic cross section, the partial pressure of the contaminant was estimated to be $\sim 10^{-3}$ of the total cell pressure. This peak was removed from the spectra by the simple expedient of drawing a smooth curve through the data on either side of the peak and subtracting the counts in the peak above this curve. Other sources of contamination from H_2 in the target could come from ^{3}He breakup producing protons or deuterons. However, for those cases where kinematics would allow such particles to add to a spectrum, their contributions, as determined from the amount of H_2 contaminant and the known or estimated breakup cross sections, were completely negligible. A D_2 contamination was also noticed in the Los Alamos runs, probably as a result of the energy calibration procedure for protons. Monoenergetic recoil deuterons were observed in the deuteron spectrum, but this peak occurred at energies above the deuteron continuum. A small artifact of this peak, which leaked into the proton spectrum, was easily accounted for in the data reduction. In general, estimates of contamination of the various particle spectra by reactions of ^{3}He with the very small amount of D_2 showed that such contributions were negligible; however, some small number of counts in the triton spectra occurring at channels above the triton continuum may be attributed to these processes. In any case, these were eliminated by subtracting a (small) flat background from the triton spectra guided by the counts above the continuum.

Other features in the proton spectra were studied to see if any other contaminants might be present. A disturbing feature was a sharp break in the low energy region, seen at channel 50 in Fig. 3. An attempt to correlate this with various of the breakup reactions of ^{3}He + ^{3}He, where maximum energies are indicated by the arrows, failed when it was noted that this feature remained constant in pulse height regardless of the detector angle, unlike the structure near channel 70 (Fig. 3), which does appear to be associated with protons from $^3\text{He} + {}^3\text{He} \rightarrow {}^3\text{He} + \text{d} + \text{p}$. The break near channel 50 has been identified as being caused by a dead layer between the ΔE and E detectors in the proton telescope. Such a dead layer will distort the shape of the spectrum but will not alter the total number

of counts. Consequently, its effect was ignored. No contaminants other than those mentioned above were discovered.

After all corrections were made, each particle spectrum was integrated from E^* to the maximum possible energy. The resulting cross sections, called σ^*, were then multiplied by $\sin\theta$ so that the integration over angle could be made. Examples of $\sigma^* \sin\theta$ are shown in Figs. 4–6 as a function of the laboratory angle θ. Figure 4 shows a comparison between some of the data taken at Minnesota and Los Alamos—deuterons at 17.9 MeV and tritons at 24.0 MeV. The Los Alamos data shown in this figure had not yet been corrected for the beam interception problem at forward angles, which is clearly worse at 17.9 than 24 MeV. Error bars shown for the Los Alamos points are statistical only, and the errors for the Minnesota data are comparable. The arrow labeled θ^*_{max} indicates the maximum possible angle beyond which none of the reactions (Table I) can contribute particles to the given σ^* integral. As a check on the method, $\sigma^* \sin\theta$ must become zero at angles greater than or equal to θ^*_{max}. Figure 5 shows $\sigma^* \sin\theta$ for protons at 17.9 and 24 MeV measured at Los Alamos. The arrow labeled θ^*_{max} is calculated for the $^3He + {}^3He \rightarrow \alpha + p + p$ reaction which produces the most energetic protons and therefore the largest value for θ^*. However, the partial cross section results reported below indicate that the (pd ^{3}He) channel makes a substantial contribution to the proton spectrum. θ^* for that reaction is also shown in Fig. 5, suggesting that the change in shape of $\sigma^* \sin\theta$ near that point is associated with termination of the (pd ^{3}He) channel.

In order to integrate over angle, the experimental values of $\sigma^* \sin\theta$, such as illustrated in Figs. 4–6, were summed as histograms from the smallest measured angle to the largest. The total error for this sum, including counting statistics and errors associated with various corrections and background subtractions, was then calculated. One must then estimate the contribution to the integral from angles outside of the measured experimental range. For the large angles, σ^* at the largest measured angle was ex-

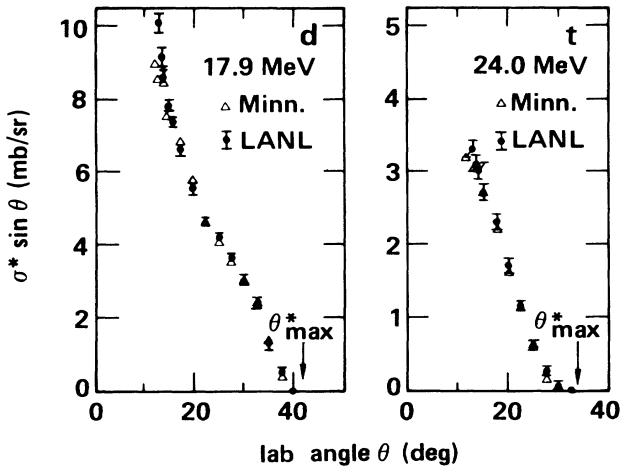

FIG. 4. Comparison of $\sigma^* \sin\theta$ for Minnesota and Los Alamos measurements for deuterons at 17.9 MeV and tritons at 24.0 MeV. The forwardmost-angle Los Alamos data were not yet corrected for the beam interception problem mentioned in the text. The arrow labeled θ^*_{max} indicates the maximum possible angle at which the indicated particle can contribute to σ^* from any allowed reaction.

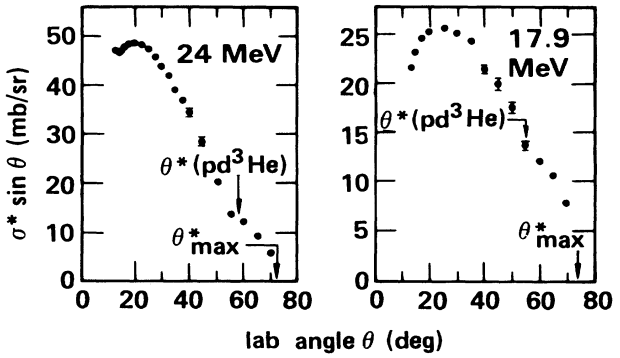

FIG. 5. $\sigma^* \sin\theta$ for protons at 24.0 and 17.9 MeV from the Los Alamos measurements. The forwardmost-angle data are corrected for the beam interception problem. The arrow labeled θ^*_{max} indicates the maximum possible angle at which protons can contribute to σ^* from any allowed reaction. The other arrow indicates the maximum possible angle for protons from the $^3He + {}^3He \rightarrow p + d + {}^3He$ reaction.

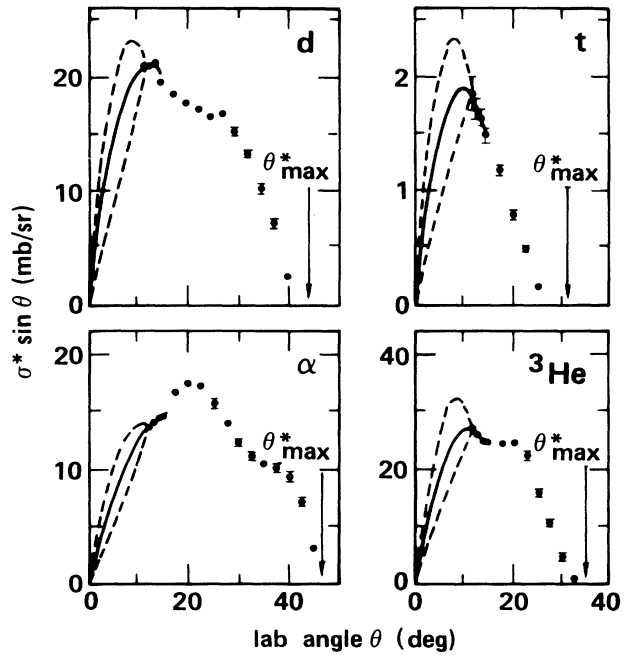

FIG. 6. $\sigma^* \sin\theta$ for deuterons, tritons, α particles, and ^{3}He particles at 21.7 MeV from the Minnesota measurements. θ^*_{max} is as defined in Figs. 4 and 5. The curves shown on each graph are the results of straight-line extrapolations of σ^* to 0° as explained in the text. The solid curve determines the small angle contribution to the angular integral, and the dashed curves are used to estimate errors in the extrapolation.

trapolated linearly to a value of zero at θ^*_{max}. This contribution was generally very small and the associated error was estimated to be negligible compared to other errors in the angular integration. The largest source of error was encountered in the forward angle extrapolation to 0°. Here the technique was to fit a straight line to the three forwardmost points on a plot of σ^* vs θ and extrapolate that line to 0°; let $\sigma^*(0)$ be the intercept of that line. To gain an estimate of the error involved, two additional lines were drawn from σ^* at the smallest measured angle to 0°—one terminated at $2\sigma^*(0)$ and the other at $0.5\sigma^*(0)$. When plotted as $\sigma^* \sin\theta$ these lines appear, for example, as the three curves shown in Fig. 6. The contribution to the angular integral is then given as the appropriate area under the solid curve, and the limits of error are taken as being represented by the dashed curves. This is the largest error in this experiment and is added in quadrature to the other errors to get the total error.

IV. RESULTS

The particle production cross sections σ_x were obtained from Eq. (11) by integrating each particle spectrum over energy and then integrating over solid angle. In all cases where separate data were obtained at the two laboratories (d, t, ^{3}He, and α at 17.9 MeV, d and t at 24 MeV) the agreement was well within the adopted errors. For these cases the σ_x values were averaged. However, because the largest source of error, the 0° extrapolation, is not independent for the two measurements, rather than combine the two errors the smallest of the two was adopted. The final production cross sections are plotted as a function of ^{3}He bombarding energy in Fig. 7.

At 17.9 MeV the total reaction cross section σ_R may be calculated from the data in two ways. Using Eq. (4) one obtains 151±4.7 mb and from Eq. (7), essentially

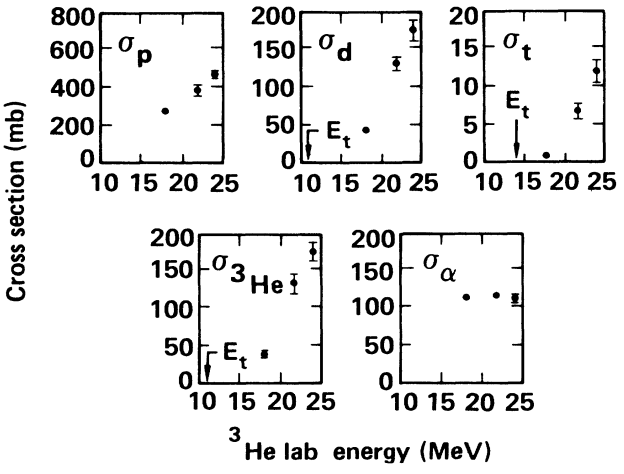

FIG. 7. Measured particle production cross sections for ^{3}He+^{3}He as a function of bombarding energy. The 21.7 MeV point for proton production was inferred from measurements of the other particles as explained in the text. The threshold energies E_t for the production of each particle are indicated by the arrows.

TABLE II. Total reaction cross section σ_R for ^{3}He+^{3}He as a function of bombarding energy. Individual reaction cross sections that comprise σ_R are also given for the various final states. Units are mb.

Cross section	17.9 MeV	21.7 MeV	24.0 MeV
σ(2pα)	112.0±4.4	114.3±4.7	110.1±6.4
σ(pd ^{3}He)	41.7±4.4	129.5±9.1	147 ±24
σ(3pt)	0.4±0.1	6.5±1.0	11.6±1.6
σ(2pn ^{3}He)	<4[a]	<16[a]	14.7±14.8
σ(2p2d)	b	b	12.8±13.7
σ_R	156.7±3.8	250 ±14	296 ±12

[a]Only an upper limit could be determined.
[b]Below threshold.

Bacher's[18] method, one obtains 159.5±4.7 mb. Because σ_t is negligible for these cases, these two methods are independent and their agreement confirms the correctness of this approach. The value adopted at 17.9 MeV is the weighted average of these two results. At 21.7 MeV, because of the lack of proton data, only Eq. (4) could be used to extract σ_R. However, with this result for σ_R, Eq. (7) can be used to calculate σ_p. This calculated value is plotted in Fig. 7. The individual reaction cross sections for 17.9 and 21.7 MeV were extracted from the production cross sections using Eq. (5) and are presented along with σ_R in Table II. For 24 MeV, Eqs. (3) and (6) were used to determine σ_R and the individual cross sections, and these are also given in Table II.

V. DISCUSSION

In Fig. 8 we have plotted our values of σ_R as a function of ^{3}He energy along with the measurements of Ref. 18

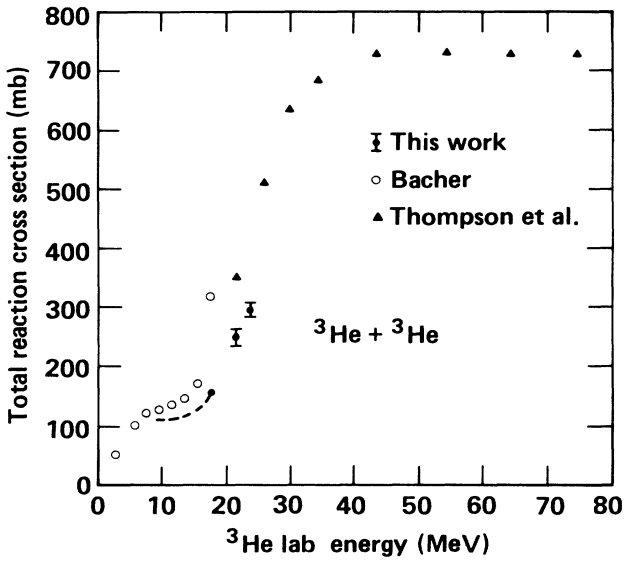

FIG. 8. The total reaction cross section for ^{3}He+^{3}He as a function of energy. The present data (solid dots with error bars) are compared with the measurements of Ref. 18 (open circles) and the RGM calculations of Ref. 12 (solid triangles). The dashed curve is an estimate of the reaction cross section based on an extrapolation of our measurements.

and the RGM calculations of Ref. 12. Although we see a sharp increase in σ_R over the range of energies we have measured, it is clearly not as dramatic as the RGM calculations indicate. Our measurements show that the $^3He+^3He \rightarrow p+d+^3He$ reaction is responsible for the increase and that the $^3He+^3He \rightarrow \alpha+2p$ reaction, which dominates at lower energies, is constant in this energy range.

We have already discussed the discrepancy with the 17.9-MeV datum of Ref. 18 and our reasons for rejecting it. In Fig. 8 we see that the trend of our data with decreasing energy does not support some of the lower energy measurements of Ref. 18 either. In Ref. 20, two 20° proton spectra from the Ref. 18 work are shown, one at 9.94 MeV and another at 15.56 MeV. In the higher energy spectrum the same prominent peak which was the cause for rejecting the 17.9-MeV data is also seen, and there even appears to be a slight hint of it at a proton energy of about 6 MeV in the 9.94-MeV spectrum. We are suspicious, then, of these data, although the alleged problem seems to disappear as the bombarding energy is reduced.

We may use the results of the present experiment to estimate σ_R at lower energies. As one goes below 17.9 MeV, $\sigma_{^3He}$ decreases to zero at the (pd ^{3}He) threshold (see Fig. 7) and only the ($2p\alpha$) channel contributes. Assuming the latter cross section is constant at the average of the values reported in Table II and extrapolating $\sigma_{^3He}$ to zero at the threshold, we generate the dashed curve shown in Fig. 8. Within errors, this curve approaches Bacher's measurements[18] at around 10 MeV. Therefore, we propose that the results of Ref. 18 below 10 MeV, along with our measurements reported here, be used as an aid in determining the phenomenological imaginary potential in future RGM calculations of the $^3He+^3He$ interaction.

ACKNOWLEDGMENTS

We thank A. D. Bacher for helpful discussions. This work was performed under the auspices of the U.S. Department of Energy by the University of Minnesota under Contract No. E(11-1)-1265, by the Lawrence Livermore National Laboratory under Contract No. W-7405-ENG-48, and by the Los Alamos National Laboratory under Contract No. W-7405-ENG-36.

*Present address: Measurex Corporation, Sensor Division, One Results Way, Cupertino, CA 95014.

[1]K. Wildermuth and Y. C. Tang, *A Unified Theory of the Nucleus* (Vieweg, Braunschweig, 1977); Y. C. Tang, M. LeMere, and D. R. Thompson, Phys. Rep. **47**, 167 (1978).

[2]Y. C. Tang, in *Topics in Nuclear Physics II: A Comprehensive Review of Recent Developments,* Vol. 145 of *Lecture Notes in Physics,* edited by T. T. S. Kuo and S. S. M. Wong (Springer, Berlin, 1981), p. 571.

[3]R. E. Brown, in *Clustering Aspects of Nuclear Structure and Nuclear Reactions,* Proceedings of the Third International Conference on Clustering Aspects of Nuclear Structure and Nuclear Reactions, AIP Conf. Proc. No. 47, edited by W. T. H. van Oers, J. P. Svenne, J. S. C. McKee, and W. R. Falk (AIP, New York, 1978), p. 90. This reference gives a summary of applications of the resonating group method to light systems.

[4]R. E. Brown and Y. C. Tang, Nucl. Phys. **A120**, 225 (1971); in Fig. 5 the indicated σ_R scale should be divided by 2.

[5]D. R. Thompson, Y. C. Tang, and R. E. Brown, Phys. Rev. C **5**, 1939 (1972).

[6]F. S. Chwieroth, Y. C. Tang, and D. R. Thompson, Nucl. Phys. A **189**, 1 (1972).

[7]R. D. Furber, R. E. Brown, G. L. Peterson, D. R. Thompson, and Y. C. Tang, Phys. Rev. C **25**, 23 (1982).

[8]L. F. Canto, Nucl. Phys. **A279**, 97 (1977).

[9]D. R. Thompson and Y. C. Tang, Phys. Rev. C **4**, 306 (1971).

[10]J. A. Koepke, R. E. Brown, Y. C. Tang, and D. R. Thompson, Phys. Rev. C **9**, 823 (1974).

[11]R. E. Brown, I. Reichstein, and Y. C. Tang, Nucl. Phys. **A178**, 145 (1971).

[12]D. R. Thompson, Y. C. Tang, J. A. Koepke, and R. E. Brown, Nucl. Phys. **A201**, 301 (1973).

[13]A. M. Sourkes, A. Houdayer, W. T. H. van Oers, R. F. Carlson, and R. E. Brown, Phys. Rev. C **13**, 451 (1976).

[14]G. E. Thompson, M. P. Epstein, and T. Sawada, Nucl. Phys. **A142**, 571 (1970).

[15]P. M. Hegland and R. E. Brown, Bull. Am. Phys. Soc. **23**, 500 (1978).

[16]J. A. Koepke and R. E. Brown, Phys. Rev. C **16**, 18 (1977).

[17]Unless stated otherwise, energies and angles are referred to in the laboratory frame of reference.

[18]A. D. Bacher, Ph.D. thesis, California Institute of Technology, 1967; private communication.

[19]Because E^* is independent of the reaction, this method does not depend on whether these reactions are three-or-more-body breakup reactions or whether they proceed in sequential stages.

[20]A. D. Bacher and T. A. Tombrello, Rev. Mod. Phys. **37**, 433 (1965).